Laboratory experiments on Wavestar device

Definition and comparison of hydrodynamic coefficients

Ferri, Francesco; Kramer, Morten Mejlhede

Publication date:
2013

Document Version
Publisher's PDF, also known as Version of record

S D W E D

STRUCTURAL DESIGN OF WAVE ENERGY DEVICES

Laboratory experiments on Wavestar device

Definition and comparison of hydrodynamic coefficients

Francesco Ferri
Morten M. Kramer

Deliverable D4.1

ISSN 1901-726X
DCE Technical Report No. 148

AALBORG UNIVERSITY
Department of Civil Engineering

Aalborg University
Department of Civil Engineering
Structural Design of Wave Energy Devices

DCE Technical Report No. 148

Laboratory experiments on Wavestar device

Definition and comparison of hydrodynamic coefficients

by

Francesco Ferri
Morten M. Kramer

March 2013

Scientific Publications at the Department of Civil Engineering

Technical Reports are published for timely dissemination of research results and scientific work carried out at the Department of Civil Engineering (DCE) at Aalborg University. This medium allows publication of more detailed explanations and results than typically allowed in scientific journals.

Technical Memoranda are produced to enable the preliminary dissemination of scientific work by the personnel of the DCE where such release is deemed to be appropriate. Documents of this kind may be incomplete or temporary versions of papers—or part of continuing work. This should be kept in mind when references are given to publications of this kind.

Contract Reports are produced to report scientific work carried out under contract. Publications of this kind contain confidential matter and are reserved for the sponsors and the DCE. Therefore, Contract Reports are generally not available for public circulation.

Lecture Notes contain material produced by the lecturers at the DCE for educational purposes. This may be scientific notes, lecture books, example problems or manuals for laboratory work, or computer programs developed at the DCE.

Theses are monograms or collections of papers published to report the scientific work carried out at the DCE to obtain a degree as either PhD or Doctor of Technology. The thesis is publicly available after the defence of the degree.

Latest News is published to enable rapid communication of information about scientific work carried out at the DCE. This includes the status of research projects, developments in the laboratories, information about collaborative work and recent research results.

Published 2013 by
Aalborg University
Department of Civil Engineering
Sohngaardsholmsvej 57,
DK-9000 Aalborg, Denmark

Printed in Aalborg at Aalborg University

ISSN 1901-726X
DCE Technical Report No. 148

Recent publications in the DCE Technical Report Series

ISSN 1901-726X
DCE Technical Report No. 148

Contents

1 Objectives

The main objective of the present report is to estimate the framework and to tune the coefficients of a linear dynamical numerical model representing a point absorber wave energy converter using laboratory tests. Once this task is achieved the model can be used in an advanced control strategy, which relies on the linearized dynamical model of the system. Specific objectives of this laboratory tests are to calculate and compare:

- Gravity Moment
- Inertia Coefficient
- Hydrostatic Stiffness
- Radiation Moment coefficients (Added Mass and Damping)
- Excitation Moment coefficients (Magnitude and Phase)

All of these points can be achieved by measuring the force acting on the linear motor rod, the surface elevation, and pitch motion of the system, see section 4 for more details.

2 Nomenclature

A list of acronyms and symbols used through the document are reported below,Table 1. Beside every item a brief description is given.

Table 1: Acronyms and Symbols

Symbols and Acronyms	**Description**
ACRONYMS	
WEC	Wave Energy Converter
DoF	Degree of Freedom
FRF	Frequency Responce Function
irf	Impulse Responce Function
PTO	Power Take-Off system
PDE	Partial Differential Equation
SYMBOLS	
a	Wave Amplitude, [m]
H	Wave Height, [m]
L	Characteristic body length, [m]
ξ_i	Body displacement in the i-th mode
M_{hy}	Hydrostatic Moment
M_{rad}	Radiation Moment
M_{ex}	Excitation Moment
M_{others}	General/not specified Moment
A_{ij}	Added Mass matrix coefficients relative to mode i affected by mode j
B_{ij}	Radiation Damping matrix coefficients relative to mode i affected by mode j
K_{ij}^{hy}	Hydrostatic stiffness matrix coefficients relative to mode i affected by mode j
M_i^{ex}	Excitation complex coefficients relative to mode i
ω	Rotational frequency, [rad/s]
T	Period of oscillation, case sensitive, [s]
$\Delta\theta$	Angular stroke, [rad]
θ	Angular displacement from the equilibrium or starting position, [rad]

3 Introduction

The work described in this report is a preliminary work, in order to achieve the optimal control of the wave energy converter Wavestar. The main aim of this test campaign is to validate the numerical coefficients obtained from the boundary element method (BEM) software, WAMIT, in order to calibrate the time domain model to be used in the optimal control loop 3.1. After these tests another campaign needs to be carried out in order to compare different control strategies applied in the physical model with the numerical result. Using the correct control strategy it is possible to increase the efficiency of the wave body interaction, seeking for a so called resonance condition.

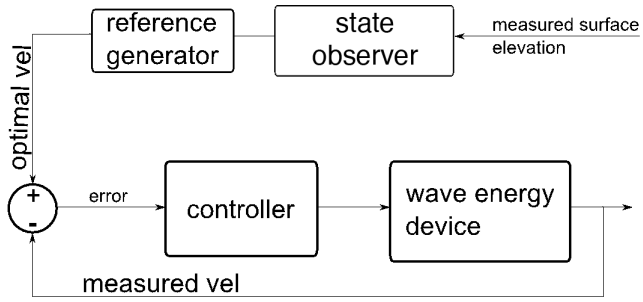

Figure 3.1: Optimal control loop

The basic idea behind this control strategy, called reactive control, is to make the flux of energy from the floater to the PTO reversible in function of the incoming force and the velocity of the system. In other words, we invest some energy into the system in order to try to increase the motion of it and therefore increase the power outtake. As shown in the picture, the controlled variable is the body velocity, which needs to be held in phase with the excitation force. The input in the closed loop controller is therefore the difference, called error, between the measured velocity and the predicted one (set point). In order to assess the error in the time domain three different steps are needed:

1. Evaluate the surface elevation at the floater position either based on the measured surface elevation in front of the device, or on the past information of the surface elevation at the device location

2. Evaluate the excitation force and use it as input for the set point evaluation, from the device dynamic model

3. Evaluate the actual error in the controlled variable

Point 1 of the list has been analyzed and further information on the method can be found in Ferri et al 2012 or Fusco et al 2010 while Point 2 is the base of work for this report. The numerical model is built from the BEM coefficients, as will be explained briefly in the background section, and since the basic assumption of the theory is small motion around the equilibrium position a calibration/check with the laboratory result is needed in order to make the numerical model match the reality. This step is required mainly for two reasons:

- The physical model is an approximation of the CAD drawing, and small differences can arise due to this discrepancy,
- The BEM coefficients are calculated from a linear theory in which the extrapolation of large motion is not only not recommended but also theoretically incorrect.

The main result shows a range of wave amplitude where the agreement between the numerical model and the calculated coefficients is satisfactory. Outside this range, as expected, the error induced by the coefficient can be higher than 100%. The main difference found in the valid region can be attribute to a summation of errors in: measurement inaccuracy, positioning and filtering. In addition to those some nonlinearities in the waves and the system itself can contribute to the empirical errors.

4 Background

The main aim of this paragraph is to explain the math behind the numerical model and where the coefficients, calculated and measured, are going to be used.

4.1 General consideration

In the marine field mainly two simple approximations are commonly used in order to describe the motion of a body affected by a wave pattern.

- Small body approximation, Morrisons equation
- Diffraction/Radiation theory, Linear Model

The dimensionless number used to switch between the equations is the Keulegan-Carpenter number (KC), which describe the relative importance of the drag force over the inertia one, equation 1

$$KG = 2\pi \frac{A}{L} \tag{1}$$

If the KG is bigger than 10, there is a flow separation and the drag forces are dominants, Morrison equation.
If the KG is less than 2, the flow is attached to the body and the diffraction/radiation forces are dominant, Linear model.
Since the Keulegan-Carpenter number for this kind of device in operational condition (only passive damping control) is close to 2, than the system can be modeled using a large body approximation. Following, the dynamic problem can be solved using a BEM method where the system is solved as linear in a surround of the equilibrium position, see section 4.2 for a brief explanation. Beside the hydrodynamic coefficients other terms are affecting the body dynamic behavior. The different moments acting on the system are described in equation 2, which represents a general form of Newtons second law.

$$J\ddot{x} = M_{hy} + M_{rad} + M_{ex} + M_{others} \tag{2}$$

where

- $J\ddot{x}$ represents the systems inertia where J is the mass moment of inertia of the system and $\ddot{x}$ its accelerations. The other terms in the equation are described below:

- Hydrostatic Moment (M_{hy}) is proportional to the angular position of the body relative to the equilibrium point. This moment is calculated as the difference between the gravity force and the buoyancy. The gain is called Hydrostatic Stiffness.

- Radiation Moment (M_{rad}) is proportional to the angular velocity and angular acceleration. This describe the moment when the system is moved in still water. The two gains are named added mass and damping coefficient respectively.

- Excitation Moment (M_{ex}) is proportional to the surface elevation with an induced phase shift. This describe the moment due to the unsteady pressure field acting on the wetted surface, when the system is hold on position. The total moment can be decomposed into Froude-Krilove moment, related to the undisturbed pressure field acting on the body wetted surface, and a diffracted moment, related to the waves diffracted from the body.

- The last term (M_{others}) in the equation represents different contribution, as power take off (PTO), mooring and second order moments as drift and viscous moment. In this part of the work the mooring and second order moments are neglected, while the PTO moment represents the quantity measured by the load cell, which is the base for the calculation of the empiric coefficients.

Equation 2 can be reshaped into equation 3, which represent the dynamic model of the system in frequency domain.

$$-\omega^2\theta(\omega)\left(J + A_{55}(\omega)\right) - i\omega\theta(\omega)B_{55}(\omega) + \theta(\omega)K_{55}^{hy} = M_{55}^{ex}(\omega) \tag{3}$$

The terms $A_{55}(\omega)$ and $B_{55}(\omega)$ represent the radiation frequency dependent coefficients, the term K_{55}^{hy} is called hydrostatic coefficient and finally the term $M_{55}^{ex}(\omega)$ is the excitation frequency dependent moment. The subscript 55 represent the pitch degree of freedom or mode 5. Section 4.3 describes the physical meaning of the different coefficients and how they can be extrapolated out from the measured parameter.

4.2 Potential Theory

In this section some bottom line ideas of the potential flow theory are reported, in order to give a short overview of the BEM used to calculate the model coefficients. The basic assumptions behind the linear potential flow theory are the following:

- Unviscid Flow
- Irrotational Flow
- Incompressible Flow

The velocity field is defined as gradient of a scalar function, called velocity potential. Once the velocity potential is defined the irrotational condition is automatically satisfy, since the curl of a gradient is always zero. Furthermore, since the system fluid is the water, also the incompressible

condition is satisfy, which in turn lead to fulfill the continuity condition (Laplace equation). The system of PDE with boundary value to be solved is reported in equation 4

$$\begin{cases} \nabla^2\phi = \frac{\partial^2\phi}{\partial x^2} + \frac{\partial^2\phi}{\partial y^2} + \frac{\partial^2\phi}{\partial z^2} = 0 & \\ \frac{\partial^2\phi}{\partial t^2} + g\frac{\partial\phi}{\partial y} = 0 & \text{on z = 0, KBC and DBC} \\ \frac{\partial\phi}{\partial n} = V_n & \text{on } S_B,\ V_n \text{ body velocity, Body BC} \\ \frac{\partial\phi}{\partial n} = 0 & \text{on z = -h, } h \text{ water depth, Bottom BC} \\ \lim_{x\to\infty}(\phi) = 0 & \text{on x = } \pm\infty\text{, Lateral BC} \end{cases} \tag{4}$$

The Body BC is further divided in two subproblem, the *radiation* and $diffraction$ problem. In the former problem V_n is the body velocity component normal to the body surface, while in the second problem V_n is zero since the system is not moving. the force and moments are evaluated from the pressure integral over the submerged surface, equations 5 and 6.

$$\vec{F} = \iint_{S_b} (p\vec{n})dS \tag{5}$$

$$\vec{M} = \iint_{S_b} p(\vec{r}\times\vec{n})dS \tag{6}$$

The pressure p can be obtained from the linearized Bernoulli equation, once the PDE is solved and the value of ϕ is known in the whole fluid domain, equation 7

$$p = -\rho\frac{\partial\phi}{\partial t} - \rho g z = -\rho\left(\frac{\partial\phi_r}{\partial t} + \frac{\partial\phi_i}{\partial t} + \frac{\partial\phi_d}{\partial t}\right) - \rho g z \tag{7}$$

In the former equation the potential operator has been decomposed in the different problems which contribute to the main one. These are respectively, incident (i), radiated (r) and diffracted (d) problems. Therefore, even the forces and moment can be split in the same way, as presented in equation2. It is common use to sum up the diffracted and incident forces and moments in the excitation ones.

4.3 Coefficients extrapolation

Measured values need to be elaborated in order to obtain the researched coefficients. This section gives some general remarks about the coefficients extrapolation. The coefficients can be obtained basically once the overdetermined linear system of equation, define in the form $Ax = b$, is solved, where A is $[nxm]$ matrix of the independent variable/s, x is $[mx1]$ vector of unknown coefficient/s and b is a $[nx1]$ vector of the dependent variable. The number of observation is n, which is normally bigger than the number of unknowns, m. The solution can be searched using the least square criterion. When the number of unknowns is 1, the system can be solved by a simple division and calculation of the mean value of the resultant vector.

4.3.1 Gravitational Moment

The gravitational moment is the load acting on the structure due to the presence of the earths gravitational field. Since the body can be represented as a point mass concentrate at the CoG, then the gravitational moment is the product of the body weight, which is vertical orientated, times the horizontal distance (l) between the point of rotation and CoG. The dynamic equation of an oscillator in air can be described in equation 8

$$lmg + J\ddot{\theta}(t) = M_m(t) \tag{8}$$

If the test is run in quasi static condition, the term $J\ddot{\theta}(t) \approx 0$ and therefore M_m is directly the moment induced by the gravity field. The moment arm is the horizontal projection of the distance of the CoG from the rotational point, and it is a function of the actual angle, between the floater beam and the absolute horizontal line.

4.3.2 Moment of Inertia

The moment of inertia is the measure of the objects resistance to any change in its state of rotation. When the system moves with a non-zero acceleration, then the inertia term in equation 8 is not negligible any longer and the M_m is a combination of both loads. Therefore, in order to assess J, the gravitational moment need to be subtracted from the measured one. The result is the dependent variable vector, where the dimension of the vector is given by the number of observations. The independent variable is the acceleration of the body, obtained from the measured position at each sample time.

4.3.3 Hydrostatic Stiffness

The restoring moment, acting on body dip into a fluid, is the balance moment between gravitational and buoyancy moment. If the body shape is regular the restoring moment can be linearized around the equilibrium position and the derived gain is often called hydrostatic coefficient. The dynamic behavior of a body dipped in water is described by equation 9

$$J\ddot{x} = M_{hy}(t) + M_{rad}(t) + M_{ex}(t) + M_m(t) \tag{9}$$

If the period of the motion is slow enough, then the acceleration and velocity related terms become negligible, read inertia and radiation moment tend to zero. Furthermore, if the water is calm the excitation moment is zero too. Therefore, the measured moment, which is the dependent variable, is proportional to the system angular position, which is the independent variable.

4.3.4 Radiation Added Mass and Damping

The radiation moment is induced into the system when the device is moved in undisturbed water. This moment is composed by two terms, one proportional to the velocity (damping) and

one to the acceleration (added mass) of the system. These two gains are frequency dependent and therefore it is possible to obtain them moving the system at different frequency. In case of regular harmonic motion the radiation moment can be defined by equation 10

$$M_{rad}(t) = A_{55}(\omega)\ddot{\theta}(t) + B_{55}(\omega)\dot{\theta}(t) \tag{10}$$

M_{rad} can be extrapolated from the M_m, if the inertia and restoring moment are subtracted to it. Therefore, the dependent variable is $M_m M_{inertia} - M_{restoring}$, the independent variables are the velocity and the acceleration of the body and the number of unknowns is two.

4.3.5 Excitation force magnitude and phase

The excitation moment is defined by the dynamic pressure field around the body wetted surface, when the body is not free to move. The excitation moment is defined for regular waves by equation 11

$$M_{ex}(t) = a\Im\{M_{ex}(\omega)e^{e\omega t}\} \tag{11}$$

Expanding all the terms in the equation it is possible to obtain the excitation moment in function of the measured surface elevation as described in equation 12

$$M_{ex}(t) = \eta(t)\Re\{M_{ex}(\omega)\} + \frac{1}{\omega}\dot{\eta}(t)\Im\{M_{ex}(\omega)\} \tag{12}$$

Furthermore, holding equation 3, when there is no motion in the system the M_m is directly the measurement of the excitation moment. Therefore, also in this case it is possible to define a linear system in order to assess the two coefficients.

Figure 5.1: Artistic representation of Wavestar WEC full scale

5 Set-up

The device under study is a physical model of the patented WEC named Wavestar.
Wavestar is a wave activated body top hinged point absorber, composed by a floater, a connection beam to a fixed structure and a power take off system, see Figure 5.1 The floater is shaped from a hemisphere and a truncated cone. The connection between the fixed structure and the floater is constrained to a rotational degree of freedom (pitch, mode 5), by the mean of a rotational bearing. The power take off (PTO) system grasp the relative motion between the fixed structure and the floater and convert it into a different kind of energy, mainly pressure if a hydraulic PTO is on duty. The physical model has been scaled using the Froude scaling factor, commonly used in hydrodynamic and some changes as been introduced into the model in order to make it feasible in laboratory scale:

- The beam, which has a specific shape in the full scale device, has been replaced by a square section aluminum beam, in order to make the system light enough and do not change drastically the center of gravity position.
- The hydraulic PTO has been replaced by a linear electrical motor, LinMot P01, and the hinging point has been moved behind the rotational bearing.

A schematic representation of the system used in laboratory is shown in Figure 5.2 As mentioned, the tests will focus on the definition of the Inertia moment, Hydrostatic Stiffness, Added Mass, Damping and Excitation moment for a single floater, scale $1 : 20$ relative to the prototype installed in Hanstholm, Denmark. The system has been equipped with the following instruments:

- Wave gauges (WGs) ♯5: measuring the surface elevation [m], resistive type
- S-Beam load cell: measuring the force acting on the linear motor [N], Futek LSB302

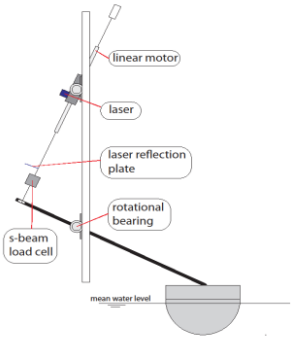

(a) Model and instrumentation sketch

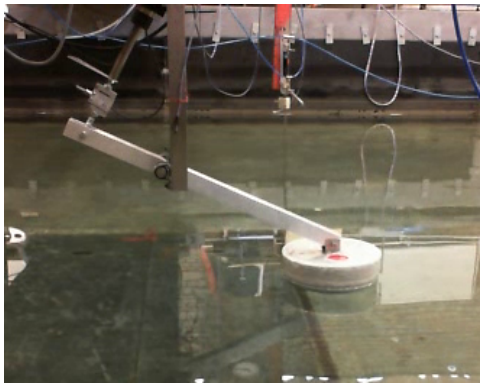

(b) Model installed in the wave basin

Figure 5.2: Wavestar physical model, scale 1:20

- Laser: measuring the displacement of the linear motor and therefore the angular motion [m], MicroEpsilon ILD-1402-600
- Linear electrical motor: PTO and control system actuator with relative controller, LinMot Series P01-37x240

The device is composed by the floater, a squared section beam, two rotational bearing, a linear motor and relative controller and a metal frame to fix the device to a bridge mounted over the basin. The WGs and floater position are represented in Figure 5.3 The data acquisition and the device control are made by Matlab-Simulink toolbox, using the xPc target to connect the host PC and the device. A cascade controller scheme was used. In particular the outer controller is defined within the Simulink block diagram, while the inner controller is a commercial micro-controller specific for the LinMot linear actuator. The Target computer collects and logs the measured data, and meanwhile it is sending the reference point for the inner controller, based on the actual state of the device. The connection flow diagram, relative to the xPC, is shown in Figure 5.4. The sample frequency for the tests has been set to 1000 Hz, in order to have an accurate time description for the controller. The system can work in position or force control. In all the tests, except the excitation ones, the system has been working in position control. The force control set-up becomes useful in a normal operational case, when the set-point is defined in terms of forces The generation of the time series for the controller is described in section 6.

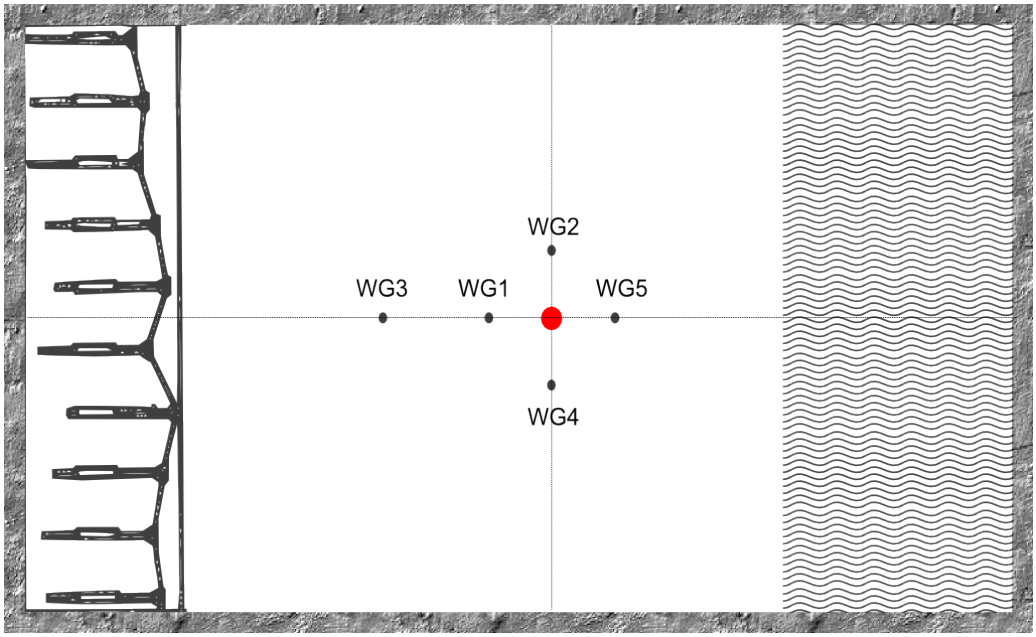

Figure 5.3: Wave basin lay-out: black dots represent wave gauge positions, red dot floater position. The snake type wave maker is represented on the left hand side while the gravel beach on the right side

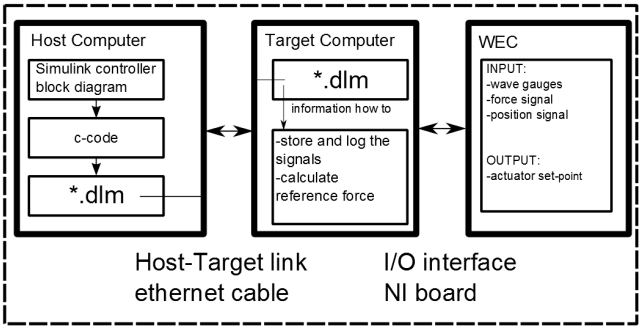

Figure 5.4: xPC Target general layout

6 Test Description

In total 89 tests have been run in order to check the BEM coefficient and 173 using a linear control strategy or other purpose. 12 tests were run in air and 77 in water. The tests in water were divided into still water or radiation tests and waves or excitation tests. The devices motion can be controlled using the LinMot (inner) controller, setting the controlled variable to be ether the position or force. During the tests with motion in air or still water, the system was controlled through its position, while for the tests in waves the controller was turned off and the systems locked at the equilibrium position. When the controller was operative, the reference position signal was build as following:

- 2*T starting region with gain set to zero
- 1*T step-up region using a cosine function
- 8*T steady region
- 1*T step-down region

for a total signal length of 12*T seconds. Where T represents in this case the period of the body motion. The signal is therefore composed by 4 sections, where the first one is used to measure instrument offsets, the second and the last are used to ramp up/down the motion to/from its steady value and the third is the useful or steady state region, where the empirical coefficients are extrapolated. Both the transition sections use a Tukey window function in order to avoid abrupt acceleration on the system. This expedient shows a substantial increase of the force signal quality in the steady region. During the tests in waves, these were generated using an in-house software, AwaSys, which send the request time series to the hydraulic system which leads the paddles motion. The regular case test duration was set to 45s, while the irregular one is defined by the wave peak period. The signal generated by Wavelab has the same 4 section described previously. The Table 2 summarize the tests in air where the system was driven by the reference position function of time, and the harmonic parameter of the motion are the period, (T) and the angular stroke, ($\Delta\theta$) of oscillation. This last was converted into a linear stroke, and from it into a time series, which is the set-point time vector for the inner controller. The measured outputs of these tests are the displacement of the linear motor and the force acting on it. These two values can be converted into the relative moment and (θ) using the geometry of the model.

Table 2: Tests in air with sinusoidal oscillation, period (T) and stroke ($\Delta\theta$)

Test Name	**T[s]**	$\Delta\theta$**[rad]**
$RA04air$	0.7	01
$RA11air$	0.7	0.35
$RB04air$	1	0.1

Continued on next page

...continued from previous page

Test Name	**T[s]**	$\Delta\theta$**[rad]**
$RB11air$	1	0.35
$RC04air$	1.4	0.1
$RC11air$	1.4	0.35
$RD04air$	2	0.1
$RD11air$	2	0.35
$RE04air$	30	0.1
$RE11air$	30	0.35
$RF04air$	0.5	0.1
$RF11air$	0.5	0.35

The Table 3 summarize the tests in still water, where the system was driven by the reference position function of time, and the harmonic parameter of the motion are the period, (T) and the angular stroke, ($\Delta\theta$) of oscillation. The measured outputs of these tests are the surface elevation at the WGs position, the displacement of the linear motor and the force acting on it.

Table 3: Tests in still water with sinusoidal oscillation, period (T) and stroke ($\Delta\theta$)

Test Name	**T[s]**	$\Delta\theta$**[rad]**
$RA01rad$	0.7	0.025
$RA02rad$	0.7	0.05
$RA03rad$	0.7	0.075
$RA04rad$	0.7	0.1
$RA05rad$	0.7	0.125
$RA06rad$	0.7	0.15
$RA07rad$	0.7	0.175
$RA08rad$	0.7	0.2
$RA09rad$	0.7	0.225
$RA10rad$	0.7	0.25
$RA11rad$	0.7	0.35
$RB01rad$	1	0.025
$RB02rad$	1	0.05
$RB03rad$	1	0.075
$RB04rad$	1	0.1
$RB05rad$	1	0.125
$RB06rad$	1	0.15
$RB07rad$	1	0.175
$RB08rad$	1	0.2

Continued on next page

...continued from previous page

Test Name	**T[s]**	$\Delta\theta$**[rad]**
$RB09rad$	1	0.225
$RB10rad$	1	0.25
$RB11rad$	1	0.35
$RC01rad$	1.4	0.025
$RC02rad$	1.4	0.05
$RC03rad$	1.4	0.075
$RC04rad$	1.4	0.1
$RC05rad$	1.4	0.125
$RC06rad$	1.4	0.15
$RC07rad$	1.4	0.175
$RC08rad$	1.4	0.2
$RC09rad$	1.4	0.225
$RC10rad$	1.4	0.25
$RC11rad$	1.4	0.35
$RD01rad$	2	0.025
$RD02rad$	2	0.05
$RD03rad$	2	0.075
$RD04rad$	2	0.1
$RD05rad$	2	0.125
$RD06rad$	20.15	
$RD07rad$	2	0.175
$RD08rad$	2	0.2
$RD09rad$	2	0.225
$RD10rad$	2	0.25
$RD11rad$	2	0.35
$RE11rad$	30	0.35

The Table 4 summarize the tests in waves, the system was hold at the equilibrium position, locking the rod of the linear motor. The wave parameters are the period of oscillation, (T or Tp) and the wave height, (H or Hm0). The waves have been generated using Awasys. On the software UI the following parameters were specified: the wave height and period, the time series length and the spectrum type in the irregular case. In all the cases the wave direction have been kept fix at 0 degree, while the duration of the test was fixed for the regular case, 45s, and variable for the irregular case, in function of Tp. The time series of the surface elevation in the last case has been obtained from a JONSWAP spectrum, with a peak enhancement factor of 3.3. The outputs of these tests are the surface elevation at the WGs position and the force acting on the load cell.

Table 4: Tests in waves with fixed floater, wave period (T) and wave height (H)

Test Name	**T[s]**	**H[m]**
$RA01ex$	0.7	0.02
$RA02ex$	0.7	0.04
$RA03ex$	0.7	0.06
$RA04ex$	0.7	0.08
$RB01ex$	1.0	0.03
$RB02ex$	1.0	0.06
$RB03ex$	1.0	0.09
$RB04ex$	1.0	0.12
$RB05ex$	1.0	0.15
$RB06ex$	1.0	0.18
$RC01ex$	1.4	0.05
$RC02ex$	1.4	0.10
$RC03ex$	1.4	0.15
$RC04ex$	1.4	0.20
$RC05ex$	1.4	0.25
$RC06ex$	1.4	0.30
$RD01ex$	2.0	0.07
$RD02ex$	2.0	0.14
$RD03ex$	2.0	0.21
$RD04ex$	2.0	0.28
$RD05ex$	2.0	0.35
I$RA01ex$	1	0.031
I$RA02ex$	1.25	0.046
I$RA03ex$	1.5	0.061
I$RA04ex$	2	0.09
I$RA05ex$	3	0.144
I$RB01ex$	1	0.062
I$RB02ex$	1.25	0.092
I$RB03ex$	1.5	0.122
I$RB04ex$	2	0.18
I$RB05ex$	3	0.288

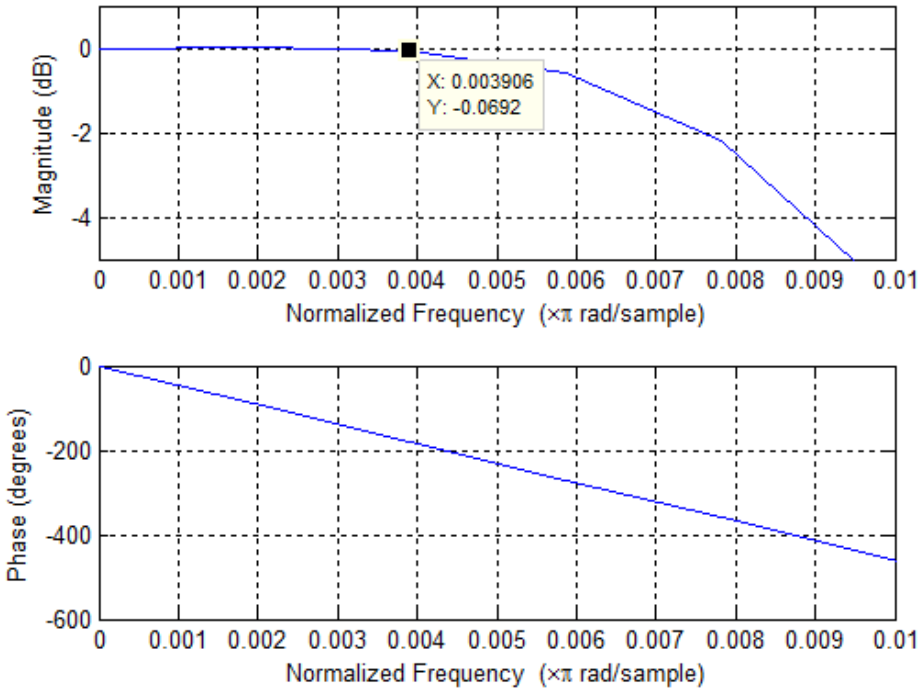

Figure 7.1: FIR filter frequency response. Magnitude and Phase coefficients in function of the normalized frequency. The point label represent the normalized cut-off frequency

7 Results and Discussion

In this chapter the results are reported and discussed using the same of structure defined in the section: Objectives, preceded by some general considerations. The first consideration is related to the calculation of the angular position, velocity and acceleration. The measured signal is a linear displacement converted to a rotational motion by geometrical relations. In order to evaluate the related velocity and acceleration the position need to be differentiates once and twice. The finite difference approximation used to obtain first and second derivative is conditioned by signal noise. Typically, the noise is amplified through each differentiation, leading to an useless set of data. In order to get rid of this problem the velocity and acceleration needs to be filtered or similarly a higher order scheme of differentiation need to be used. In particular, this process has been taken off line using Finite Impulse Response (FIR) digital low-pass filter. Since the expected maximum frequency is below 1.5Hz, and in order to limit the filter effects as phase delay and amplitude reduction the cut-off frequency has been set to 5Hz. This should ensure no influence in the frequency range of the expected motion as shown by the filter's bode diagram, Figure 7.1 The figure show that for a frequency of 1.90Hz (0.004 normalized frequency) the filter magnitude tends to zero and therefore for each frequency below it the signal has no modification of the amplitude. On the other hands, the force signal shows another prevalent frequency besides the main ones, at 5-6 Hz and therefore the same filter

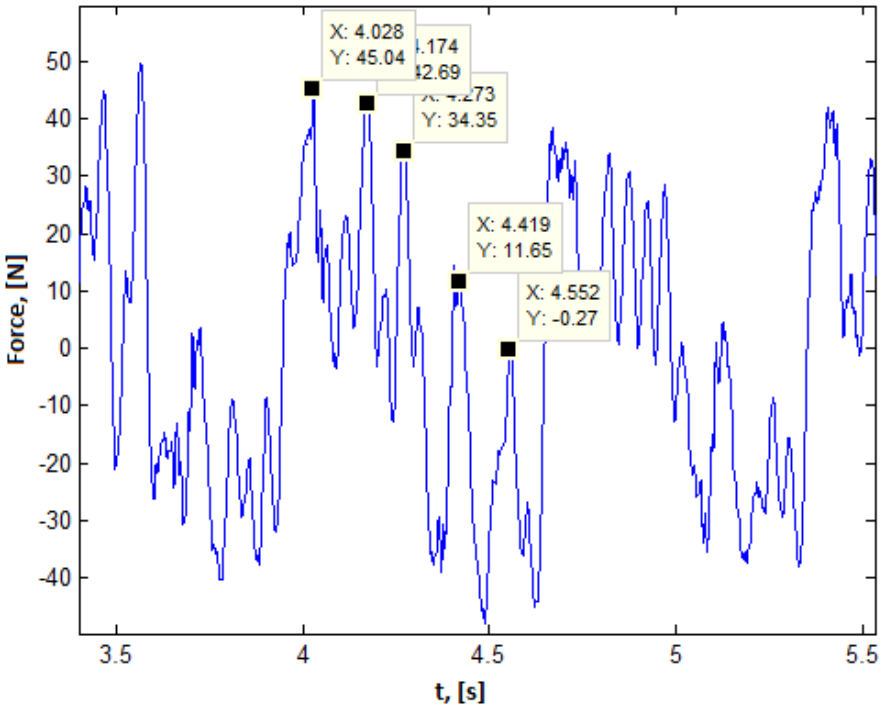

Figure 7.2: Structural vibration and its effect on the force signal. Labels represent 5 consecutive peaks

applied previously become useless in this case. The secondary frequency is basically related with the systems set-up. In fact, when the floater is forced to move in otherwise still water the "reference structure" start to vibrates at is own natural frequency. From the measured signal it is possible to estimate that frequency to be approximately 5-8Hz, as shown in Figure 7.2 The usage of a low-pass filter with the cut-off frequency of 5 Hz can be not enough to remove the effect of the structural vibration, while on the other way around, the reduction of the cut-off frequency below that value can affect the true signal related to the waves/motion. In order to get rid of this problem the best solution founded is to use a higher order FIR filter, which can ensure a sharp roll-off band and therefore less effect on the pass band. The Figure 7.3 shows how the order of the filter affects the roll-off and the pass-band. Finally the filtered result is plotted in Figure 7.4 where different types of filter have been tested.

The optimal set-up founded for the filter is the following:

- Cut-off frequency 4 Hz
- Filter Order 1024 points

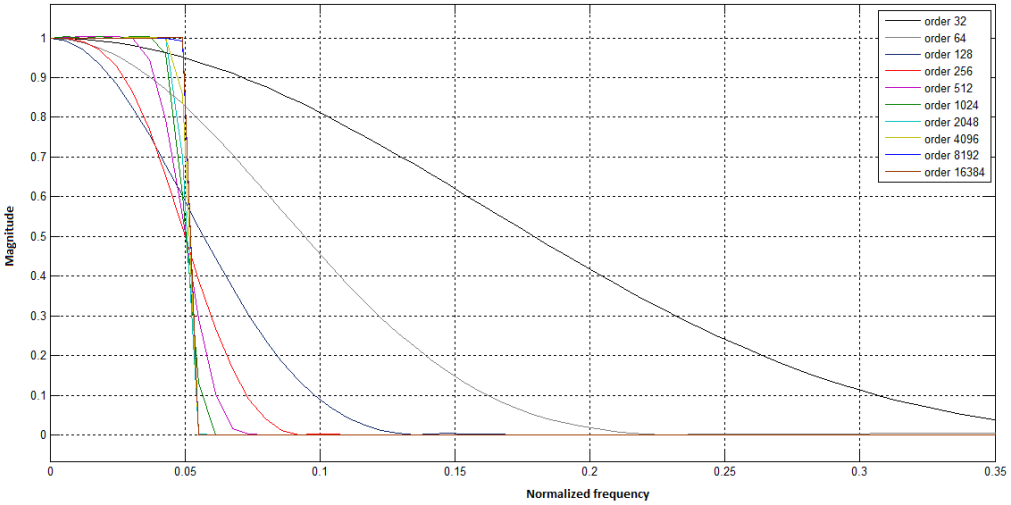

Figure 7.3: Filter roll-off behavior for 10 different filter orders

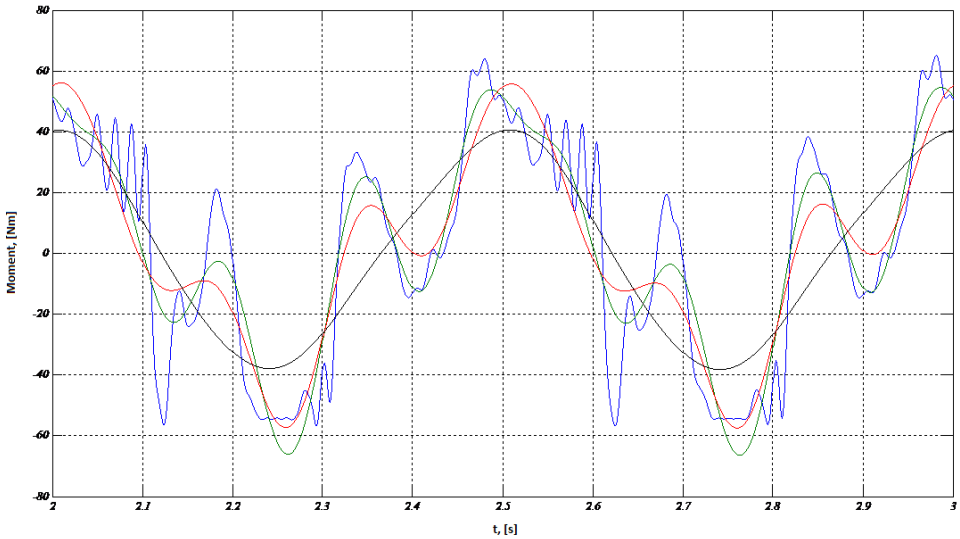

Figure 7.4: Filter output for four different cut-off frequencies (fc): fc = 100 Hz (blue line), fc = 10 Hz (green line), fc = 8 Hz (red line), fc = 4 Hz (black line)

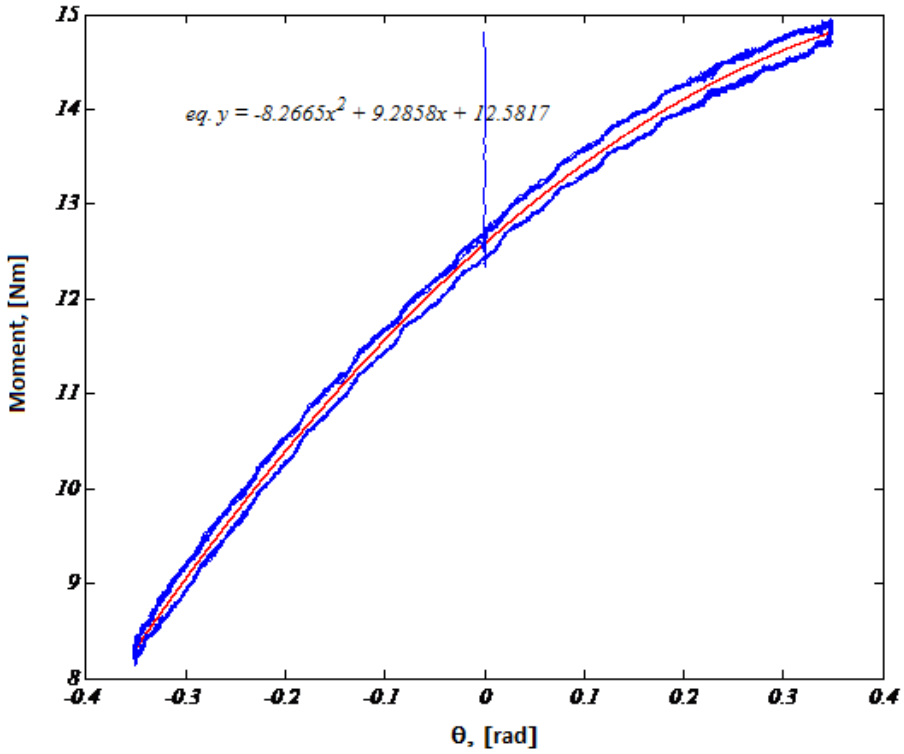

Figure 7.5: Measured moment in function of θ: Data points (blue dots) and interpolation polynomial (red line)

7.1 Gravity Moment

The knowledge of the gravity moment is request in the evaluation of the Inertia coefficient, since in air the only moments acting on the system are the inertia moment, the gravity moment and the control moment (measured/reaction moment). When the acceleration of the system is small the gravitational moment is dominant and therefore the measured force can be attributed to it. The test RE11air is used for this purpose. The system has been oscillated with a period of 30 s and an angular stroke of 0.7 rad. The Figure 7.5 shows the measured moment vs $\theta(t)$ and the corresponding interpolation coefficients. In the y axis is reported the moment due to the weight and in the x axis the angular displacement θ. Caused by the large amplitude of the motion the curve is not linear but has a sinusoidal behavior. The hysteresis of the signals can be attributed to the friction of the system, localized in the bearings. The best fitting curve in the angle range is a quadratic one and the equation of the interpolating is reported either below or in the plots area.

$$M_g = -8.27\theta^2 + 9.28\theta + 12.58 \tag{13}$$

7.2 Moment of inertia

Using the former interpolation process and changing the period of the forced oscillation it is possible to evaluate the moment of inertia of the system. Since the acceleration is not negligible any longer, as in the former test, the measured force needs to be correct by the moment due to gravity. Figure 7.6 shows the complete interpolation process for one test case while the full analysis is resumed in Table 5.

Table 5: Moment of Inertia (J) calculated for different frequencies and amplitudes of motion

Test Name	$J[kgm^2]$
RA04air	0.966
RA11air	0.996
RB04air	0.927
RB11air	0.956
RC04air	0.927
RC11air	0.943
RD04air	0.8768
RD11air	0.935
RF04air	0.990
RF11air	0.971
Mean Value	0.949

Figure 7.6 reports the different steps used to obtain the data for the fitting. The acceleration has been calculated from the position following the former described procedure. The gravity moment was subtracted from the total measured moment and the central range of the signals was selected; the starting and ending points have been removed due to the transition regions (Figure 7.6 (a-b), highlight curves). Since there is a direct proportionality between the inertia moment and the acceleration there should be no phase shift between the time series, and this is shown in Figure 7.6 (c). The last plot (Figure 7.6 d) shows the plot of the selected data (blue dots), the linear interpolating (red line) and the range of confidence (green lines) for the interpolation when a value of 2σ is chosen, where σ is the standard deviation of the process. Within the plot area it is possible to see the equation of the interpolating and the coefficient of determination which describes how well a regression line fits a set of data.

7.3 Hydrostatic stiffness (Restoring Moment)

The restoring moment is the difference between the moments due gravity and buoyancy. If the system oscillates around the equilibrium point with small amplitude the restoring moment is

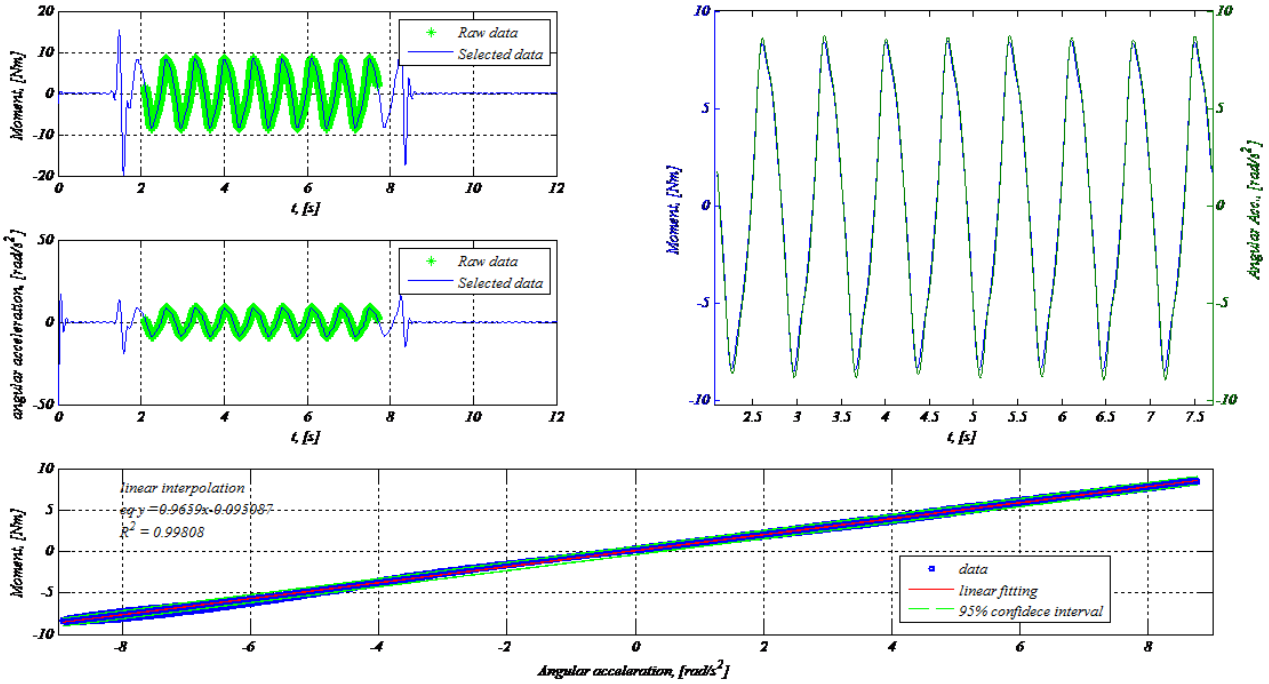

Figure 7.6: Empirical coefficient extrapolation procedure. (a-b) usable time range selection to avoid transient effects, (c) signals comparison to ensure no phase delay, (d) linear interpolation: Data points (blue dots), linear interpolant (red line), confidence intervals (green line)

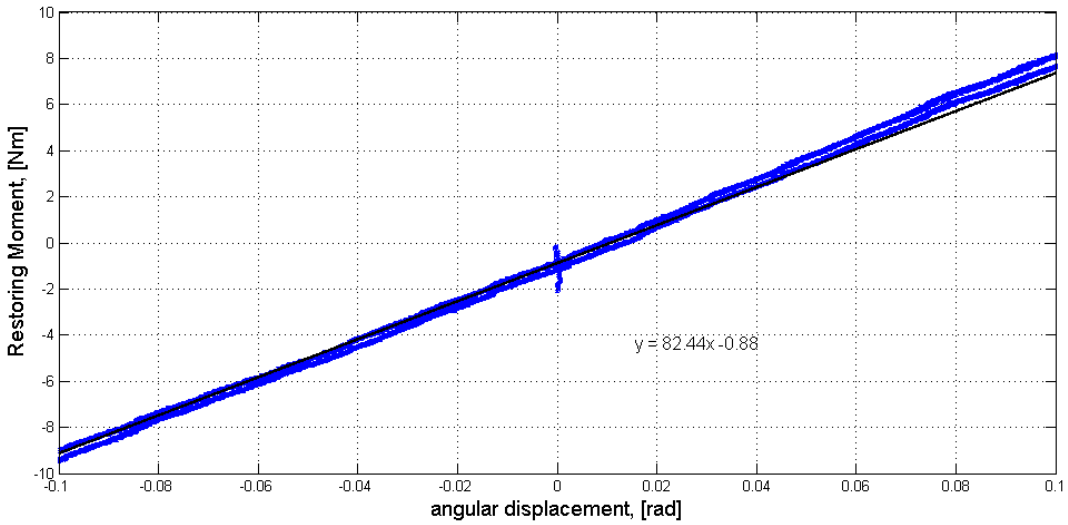

Figure 7.7: Data interpolation within a restricted range of angular displacement: data points (blue dots) and linear regression (black line) with its equation

proportional to the angular displacement. Therefore, the hydrostatic stiffness coefficient is the coefficients of proportionality between the angular position and the restoring moment, when the body is dipped in water and moved away from the equilibrium point. When a rigid body is forced to move in still water the total force is described by the sum of different force as described in the Section 4. Since the water is motionless the excitation force is zero. On the other hands, in order to make the restoring moment the dominant moment, the velocity and the acceleration of the system should be negligible. The test RE11rad is used for this purpose since an oscillating period of 30s ensures low velocity and acceleration. Figure 7.7 shows the linear interpolation of the data in a restricted range of angular displacement, while Figure 7.8 shows the trend of the force in the whole range of motion using a piecewise linear interpolation. The sharp variation of the restoring moment from the middle linear range are related to the complete submerged and complete out of water position. Figure 7.7 reports the plot of the selected data (blue dots), the linear interpolating (red line) and the range of confidence (green lines) for the interpolation when a value of 2σ is chosen, where σ is the standard deviation. The system is therefore considerable linear in the following range, -0.1:0.15 rad, which correspond to a variation in heave of -4 cm and +6 cm. It should be notice that the linear validity range is quite wide compared with the vertical body dimension, since the linear range is roughly 10 cm in heave while the body dimension is 15 cm in the vertical coordinate. Figure 7.8 shows three different linear interpolation for the three different working regions, reads out of water, normal and fully submerged. The inclination and offset of the regressions were calculated minimizing the sum of square error (sse). The measured data (blue dots) has been interpolated with three different segments, reported as red, green and black line. The same color map has been used for the respective equations. The nodes of the piecewise have been chosen to minimize the sse in the global system. The coordinate of each node is reported in the plot. Even in this case

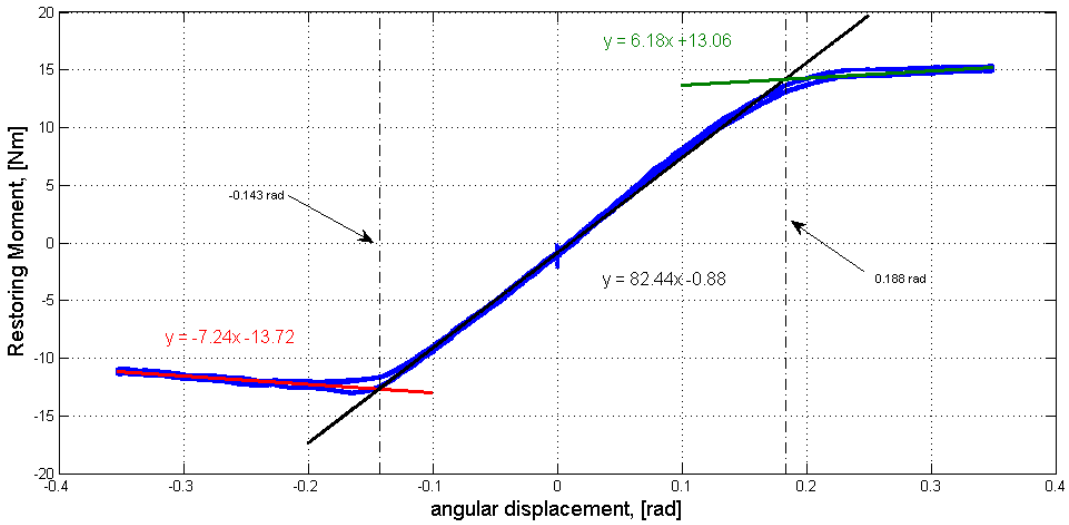

Figure 7.8: Data interpolation within the whole range of angular displacement: data points (blue dots) and linear regressions (red, black and green lines) with the respective equations. The two vertical dotted lines represent the boundary of linearity

it is possible to see some hysteresis in the force mainly ascribable to the inner friction of the system. The filtering process in this case does not seem to have any effect on the coefficients apart from the variance of the signals.

7.4 Added Mass and Damping (Radiation Moment)

Following the previous results it is now possible to extrapolate the radiation moment from the total measured force when no waves are acting on the system and both velocity and acceleration are not negligible. Since there is not a dominant moment acting on the systems, the forced motion in still water contains the contributes from the radiation, restoring and inertia moments. The radiation moment therefore can be obtained if the restoring and inertia moment are subtracted from measured one. The radiation moment is assumed to have a linear relation in both velocity and acceleration, and those coefficients (Added Mass and Damping) are changing as the frequency of the motion is changing. In order to obtain the coefficients from the extracted moment an interpolating plane have been calculated, searching for it in the least square sense. Since the radiation force is proportional to the acceleration and velocity of the body, this two time series have been calculated using the former description. The main results are reported in Figure 7.9 and 7.10 and in table A.1(APPENDIX), where the comparison between BEM coefficients and laboratory ones is shown. Figure 7.9 shows the BEM damping coefficients (gray dotted line) compared with the empirical value calculated from the lab. These are reported grouping them in function of the amplitude of the motion, where the groups specification is reported in the legend appended in the plot. Similar to the former figure, Figure 7.10 shows the comparison between the BEM added mass coefficients (gray dotted line) and the corresponding

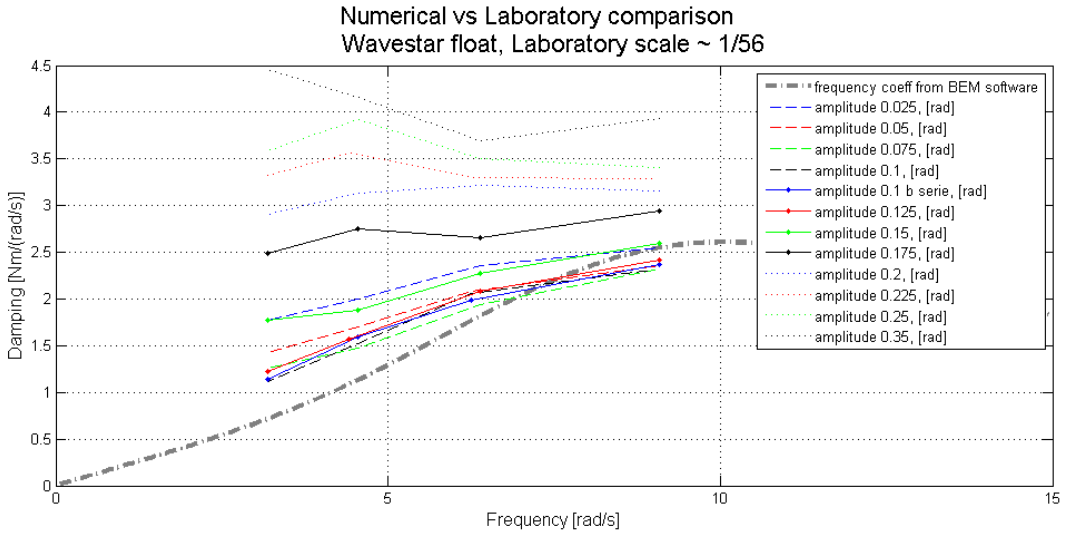

Figure 7.9: Radiation damping coefficients in function of the angular frequency: BEM coefficients (grey dotted line) and empirical coefficients clustered in function of the angular displacement. The color map used is appended in the legend

value calculated from the lab. These are reported grouping them in function of the amplitude of the motion, where the groups specification is reported in the legend appended in the plot. For the sake of of completeness the same results can be also reshaped in terms of magnitude and phase plot, Figure 7.11 and 7.12, where the magnitude is the norm of the complex frequency response function and the phase is the atan of the ratio of the real and imaginary parts. Figure 7.9 and 7.10 show a similar trend between BEM and empirical coefficients only within the intermediate range of amplitude tested. As expected the agreement gets worse as the amplitude of the motion increase, but also if the amplitude of the motion reduces. This last behaviour is against any theoretical reasons and it could only be explained by experimental errors. In fact the radiation moment is calculated by subtraction of hydrostatic and inertia moment from the measured one. Following, all the measurement errors are accumulated into a relatively small quantities, leading to a poor reliability results. On the other hands, when the amplitude of the motion is increasing the weight of non-linear behaviours, e.g. drag moment, is also increasing and therefore the linear theory underestimates the true radiation moment.
The same conclusion can be applied to the results show in Figure 7.11 and 7.12. In those plots it is even more clear how only the central range of the tested angular displacement gives a good fit between BEM and empirical coefficients. The figures show respectively the magnitude and the phase calculated from the BEM (gray dotted line) and the gain/phase obtained from the measurements. These are reported grouping them in function of the amplitude of the motion, where the groups specification is reported in the legend appended in the plot. It is important to notice how for the system under investigation the definition of god fit is not stringent, since the radiation moment is not a dominant moment. Therefore an error of 20-50 % is not affecting the overall response amplitude operator The coefficients were calculated based on a selection of the full test in order to avoid the transient region situated at the beginning and at the end

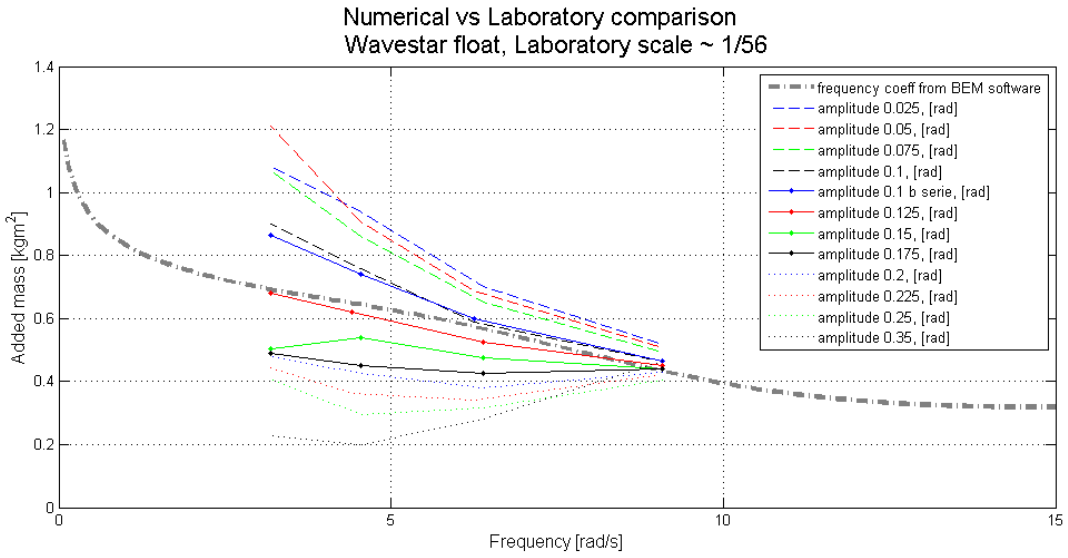

Figure 7.10: Radiation added mass coefficients in function of the angular frequency: BEM coefficients (grey dotted line) and empirical coefficients clustered in function of the angular displacement. The color map used is appended in the legend

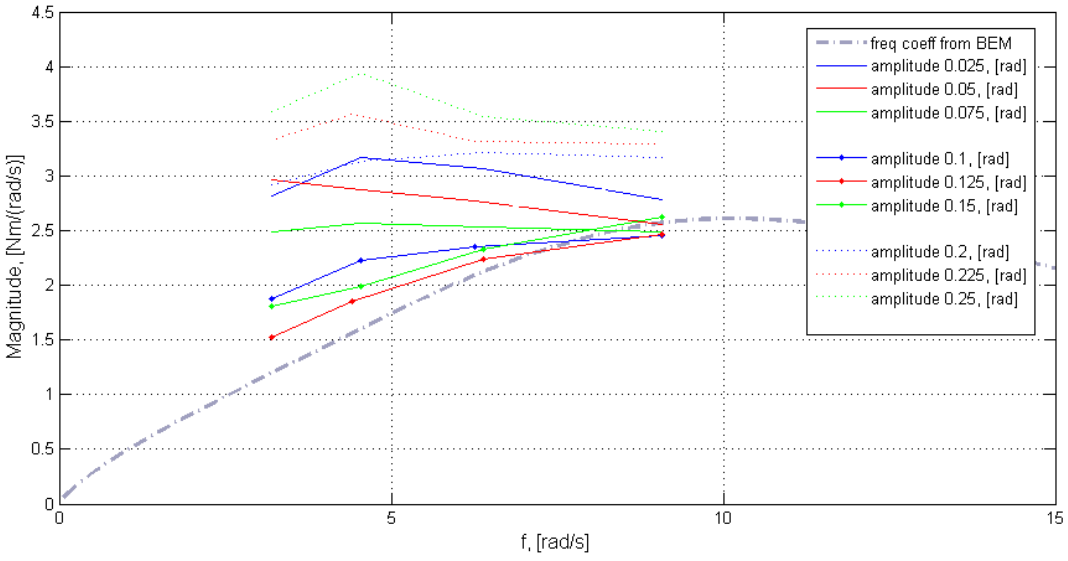

Figure 7.11: Radiation magnitude coefficients in function of the angular frequency: BEM coefficients (grey dotted line) and empirical coefficients clustered in function of the angular displacement. The color map used is appended in the legend

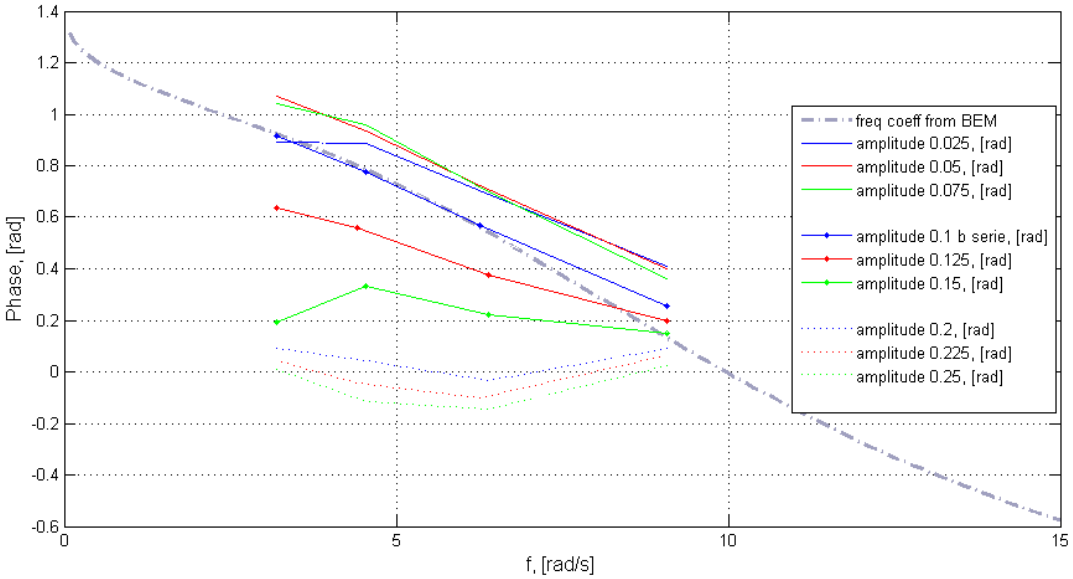

Figure 7.12: Radiation phase coefficients in function of the angular frequency: BEM coefficients (grey dotted line) and empirical coefficients clustered in function of the angular displacement. The color map used is appended in the legend

of each tests. Over 10 full oscillations only 6 were used.

7.5 Excitation Moment

The excitation moment is evaluated when the system is locked at the equilibrium position and the waves are creating a dynamic pressure filed around the wetted surface. Since there is no motion all terms related to the position, velocity and acceleration of the body drop down to zero. Therefore the measured force is directly the force due to the incoming waves and the coefficients can be calculated solving the system in the least square sense. In this case as described in the background chapter, the force is proportional to the surface elevation and its derivative divided by the frequency of the oscillation. The velocity of the surface has been obtained by derivation of the surface elevation, while the frequency has been obtained using a time domain analysis of the signal, searching for the down-crossing zeros of it. As discussed previously, the finite difference approximation used to derive the surface velocity suffer the noise amplification problem and therefore a low-pass filter was used after hand to remove the high frequency components. The same filter applied before was used in this case too. The results are shown in Figure 7.13 and 7.14. The two figures show the comparison between the numerical result (gray dotted line), and the empirical coefficients, where the dots specification is listed in the legend. Four different wave periods were tested and for each five different wave heights. In all the cases the highest wave height corresponds to the breaking limits for that period. The agreement between the BEM and empirical coefficient get worse when the wave steepness

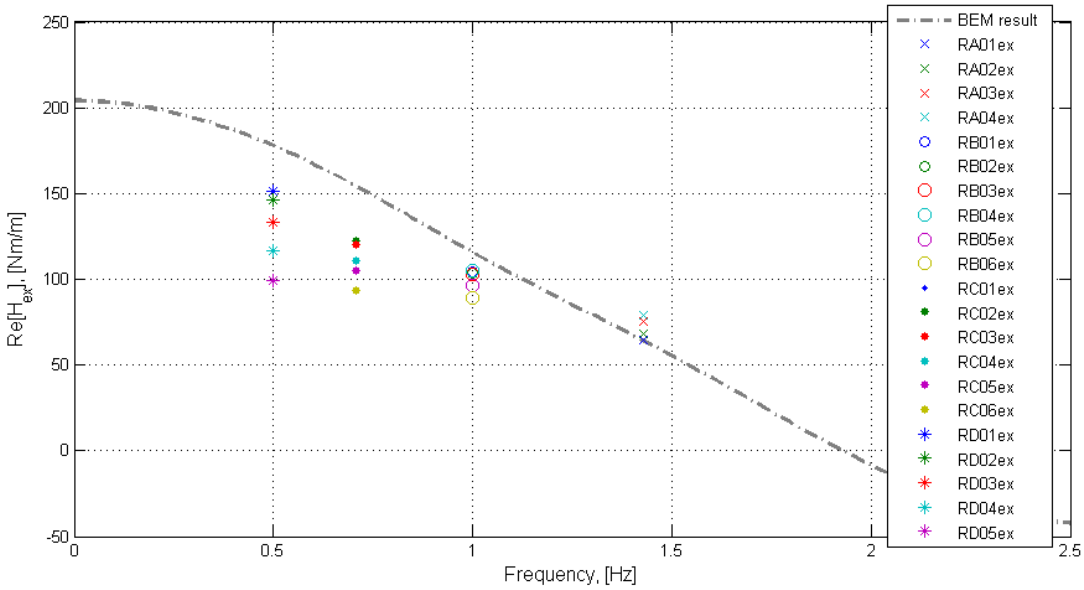

Figure 7.13: Excitation moment real coefficients in function of the wave frequency: BEM coefficients (grey dotted line) and empirical coefficients (marks) calculated from regular waves. The color map and marks types used is appended in the legend

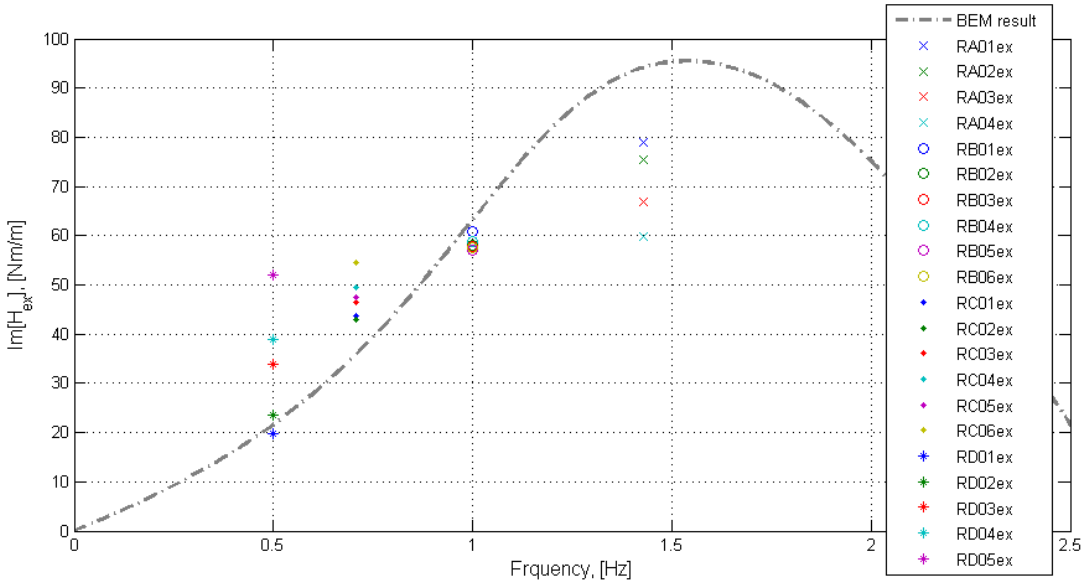

Figure 7.14: Excitation moment imaginary coefficients in function of the wave frequency: BEM coefficients (grey dotted line) and empirical coefficients (marks) calculated from regular waves. The color map and marks types used is appended in the legend

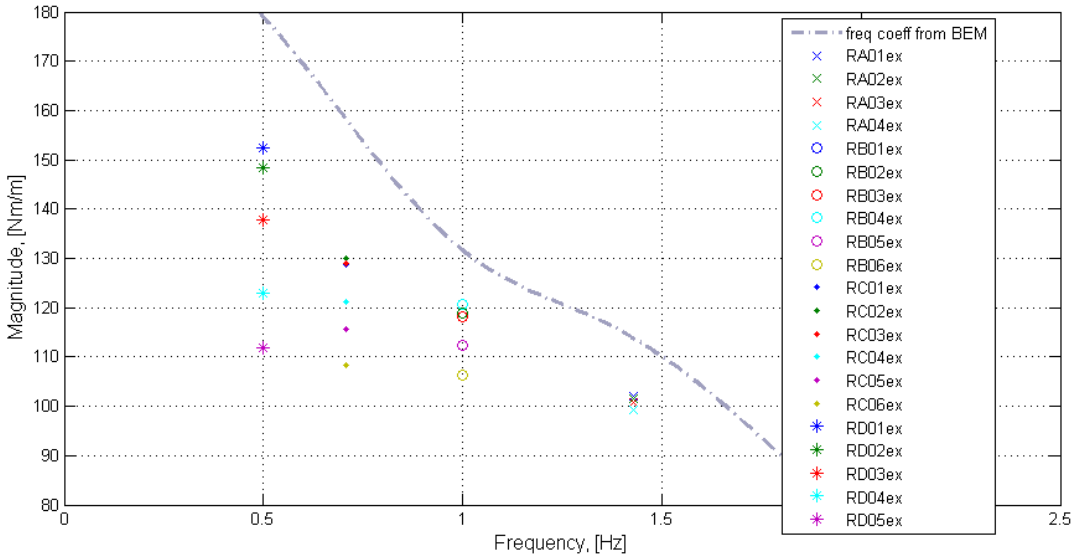

Figure 7.15: Excitation moment magnitude coefficients in function of the wave frequency: BEM coefficients (grey dotted line) and empirical coefficients (marks) calculated from regular waves. The color map and marks types used is appended in the legend

increases. The wave steepness is calculated as the ratio between wave height and wave length. This is somehow predictable from a theoretical point of view since highest steepness means also non-linear wave theory. The same results can be reshaped, as previously done, into a magnitude and phase plots. Figure 7.15 and 7.16 show these two results, where the numerical result are represented with a gray dotted line, and the empirical coefficients by dots, where the dots specification is listed in the legend. If the magnitude plot is considered, the results shows a clear trend, for which the linear model is always overestimating the true excitation moment exerted by the system. It is also important to notice how the fork within the high frequency waves is smaller than the one for low frequency. This is explained if only the overtopping is taken into consideration. In fact, since the steepness conditions were roughly constant from one period to the other, the wave height grows as the wave period become longer, until the floater gets overtopped. In this case the overtop behavior can be described as a saturation of the moment due to the limited volume of the floater. Furthermore, it is possible to obtain the excitation moment coefficients from the irregular wave cases, comparing the power spectrum of waves and moments. It should be notice that, when the power spectrum is used the phase information is lost and therefore only the magnitude of the frequency dependent excitation moment can be compared with the BEM one, Figure 7.17. The figure shows the excitation moment magnitude obtained from the BEM (gray dotted line) and the result of the wave and force power spectrums division, for low (2%) and high (4%) steepness value respectively. The results show a general agreement with the regular case tests, and they add some more detail in the range of frequency between 1 and 1.5 Hz. All the results show a peak at frequency close to the floater natural frequency (1.3 Hz). No full explanation has been found for this behaviour.

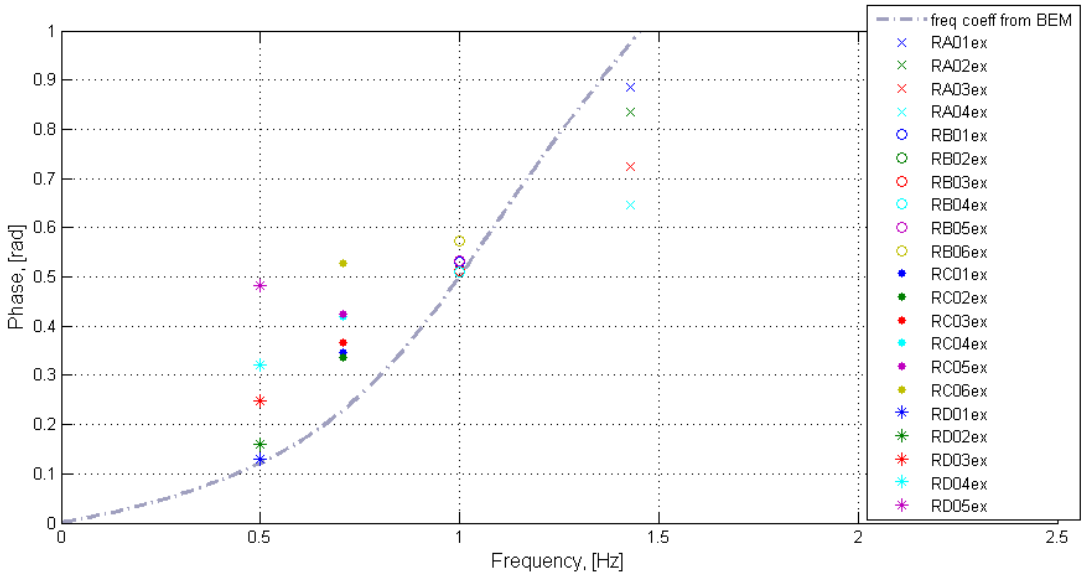

Figure 7.16: Excitation moment phase coefficients in function of the wave frequency: BEM coefficients (grey dotted line) and empirical coefficients (marks) calculated from regular waves. The color map and marks types used is appended in the legend

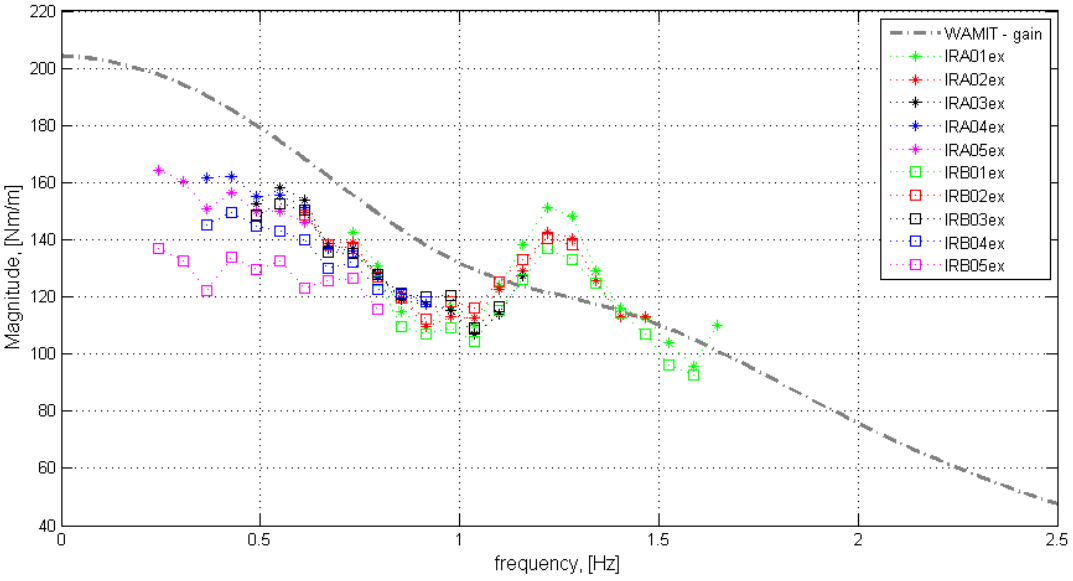

Figure 7.17: Excitation moment magnitude coefficients in function of the wave frequency: BEM coefficients (grey dotted line) and empirical coefficients (marks) calculated from irregular waves. The color map and marks types used is appended in the legend

The result for all the test are reported in the table A.2 (APPENDIX)

8 Conclusions

Aim of these laboratory tests was to obtain the model coefficients, which describe the dynamical behaviour of the Wavestar floater and compare them with the same quantities evaluated using a BEM software, WAMIT. This is the first part of a wider container where the global aim is the optimal/suboptimal control of the Wavestar device. The first result show a wide linear range for the linear hydrostatic stiffness coefficient compared with the body dimension. As described previously the linear range is valid in more than half of the body dimension. The non-linear regression is therefore necessary when the system is going to be excited with large amplitude wave or when the system is actively controlled. The short-term forecast of wave surface at the floater position can be used to evaluate the real wetted surface when the body is moving, in order to increase the accuracy of the non-linear hydrostatic force, compared with the case where only the body angle is used. Results for the radiation moment show a smaller framework, bounded at 0.125 rad. This result can be partially affected by the second order damping, since the velocity of the system for wider oscillation become important, and the viscous effect are not negligible any longer. Further investigations on the effect of the drag coefficient which represent the viscous force are planned. Finally, results from the excitation moment show over estimation of the force when the linear coefficients are used in all the frequency range if the system is excited with regular wave. Also in this case one possible cause of this behavior can be the non-linear force, mainly due to the incoming wave field. This force is known as Froude-Krylov force and can be obtained from the integration of the unsteady pressure field on the real wetted surface. Also in this case other investigations are planned. It is important to highlight, that part of the error in the excitation and radiation moment coefficient can be addressed to the order of magnitude of these force in the total one. In fact, in all the tests the main component is the hydrostatic force, and when this is subtracted to the measured moment, the remaining moment is highly influenced by measurement errors. This type of error cannot be solved since the system is basically driven by the hydrostatic moment.

9 APPENDIX

A.1

A.2

References

[1] "WAMIT Version 5.3: A RADIATION-DIFFRACTION PANEL PROGRAM FOR WAVE-BODY INTERACTIONS", DEPARTMENT OF OCEAN ENGINEERING MASSACHUSETTES INSTITUTE OF TECHNOLOGY, Year 1995.